A&A 459, 257–263 (2006)
DOI: 10.1051/0004-6361:20065512

Astronomy & Astrophysics

Observations of CN and dust activity of comet 9P/Tempel 1 around Deep Impact⋆,⋆⋆

H. Rauer[1,2], M. Weiler[1], C. Sterken[3], E. Jehin[4], J. Knollenberg[1], and O. Hainaut[4]

[1] Institut für Planetenforschung, DLR, Rutherfordstr. 2, 12489 Berlin, Germany
e-mail: heike.rauer@dlr.de
[2] Zentrum für Astronomie und Astrophysik, TU Berlin, Germany
[3] Vrije Universiteit Brussel, Pleinlaan 2, 1050 Brussels, Belgium
[4] European Southern Observatory, Alonso de Cordova 3107, Santiago de Chile

Received 26 April 2006 / Accepted 4 August 2006

ABSTRACT

Aims. We present observations of CN emission and the scattered solar light on cometary dust particles around the impact time of the Deep Space spacecraft (NASA) into the nucleus of comet 9P/Tempel 1. The purpose of the observations was to compare post-impact activity to the conditions pre-impact to search for new spectral emission lines after impact, to quantify the increase in gas activity due to the impact and to study the long-term activity changes.
Methods. We performed long-slit spectroscopy observations of comet 9P/Tempel 1 at the VLT, ESO, using the FORS instruments from July 2 to July 12, 2005. A wavelengths range of 370–920 nm was covered using two grisms. Four different position angle settings of the slit were applied each night with the projected Sun-comet line as standard setting, for which we report results here.
Results. The optical spectra of comet 9P/Tempel 1 showed the usual emission bands in the optical wavelengths range of the radicals: CN, C_3, C_2 and NH_2. No new emission bands were detected after impact. The ejecta cloud of gas and dust caused by the impacting spacecraft into the cometary nucleus could be followed over the observing period. The projected expansion velocities have been determined. The night after impact we observed about $(3.9 \pm 1.2) \times 10^{29}$ molecules of the CN parent in the ejected cloud. However, after five days the appearance of the gas and dust coma was back to pre-impact conditions.

Key words. comets: individual: Tempel 1 – comets: general

1. Introduction

Comets are studied to investigate bodies which have been modified only little since their formation during the early phases of the solar system. However, although comets have been observed intensely for a long time, we have little information about their interior. Observations of the gas and dust coma provide only indirect evidence for the nucleus composition. The Deep Impact mission (NASA) offered the opportunity to study fresh sub-surface material for the first time. On July 4, 2005, a projectile of 370 kg mass impacted on comet P/Tempel 1 with a relative velocity of 10.3 km s^{-1}. A crater was produced on the surface and a cloud of ejecta material expanded from the nucleus (A'Hearn et al. 2005). This event was observed not only from the impactor and fly-by spacecraft, but also in a world-wide ground-based observing campaign (Meech et al. 2005).

At the European Southern Observatory (ESO) two observing campaigns were performed around impact time to investigate the gas and dust components of the comet. All ESO telescopes were involved in these campaigns to provide information on the target comet in all available wavelength band passes from optical to thermal infrared. Here, we report on the first results from optical long-slit spectroscopic observations of the gas and dust component. The scientific goals of these observations were to investigate whether new emission lines would appear in the spectrum after impact, quantify the gas sublimated during and after impact, search for new active surface areas on the comet and investigate for how long the additional activity is sustained. A comparison with pre-impact conditions is made to investigate possible differences in abundance ratios of the ices in the nucleus. In this paper, we concentrate on the CN and dust activity evolution of the comet. A comparison to other radicals emitting at optical wavelengths and present in our spectra is made in a subsequent publication.

2. Observations and data reduction

The observations started on the night of July 02/03, two days before impact, and lasted until July 10 at UT1 of the VLT, ESO, using FORS 2. Two additional nights of measurements were then performed using FORS1 at UT2. During the observations, 9P/Tempel 1 was at a heliocentric distance of 1.51 AU and a geocentric distance of 0.88−0.94 AU (see Table 1). Two grisms were used at UT1, covering in total 370–920 nm. However, the red part of the spectral range, 610−920 nm, was covered only once per night, whereas the blue range was the standard setting. The resolving power is 780 for the 370–620 nm range and 660 for the 610–920 nm range, using FORS 2. For the spectra taken at FORS 1 the resolving power is 780. The slit length was 6.8′ and a slit width of 1″ was used to observe the comet. The pixel scale is 0.252″ $pixel^{-1}$ (after a 2×2 binning) in the spatial and 1.5 Å $pixel^{-1}$ in the wavelength direction for FORS 2.

⋆ Based on observations collected at the European Southern Observatory, Chile (ESO Programme 075.C-0355).
⋆⋆ Table 1 is only available in electronic form at http://www.aanda.org

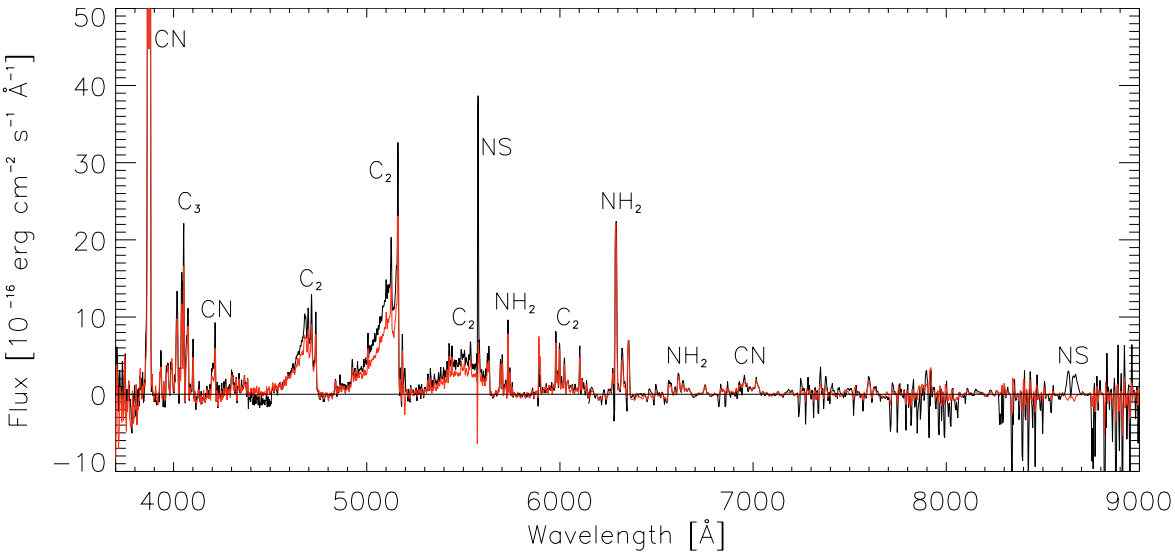

Fig. 1. Continuum subtracted spectra taken $1^h\ 49^m$ before impact (red) and $17^h\ 59^m$ after impact (black). The spectra are integrated from 0–6.5 × 10^4 km along the projected Sun direction to enhance the signal-to-noise ratio. Remnants of night sky lines are marked with NS.

For FORS 1, the corresponding values are 0.20″ pixel^{-1} and 1.2 Å pixel^{-1}. These values correspond to a pixel scale of 162.3–129.2 km pixel^{-1} for FORS 2 and 135.2–135.9 km pixel^{-1} for FORS 1, respectively. The detector of the FORS 2 instrument consists of two individual 2048 × 4096 pixel CCDs which are separated by a gap of 480 μm, corresponding to 4.03″. The gap is parallel to the wavelength direction. The FORS 1 instrument uses a single CCD with 2048 × 2048 pixels.

The position angle of the projected solar direction ranges from 291.7° on the evening of July 2, 2005, to 290.3° on the morning of July 12. The slit was oriented at four different position angles, the reference position being along the Sun-comet line. The additional spectra were taken perpendicular to the Sun-comet line and at 45° angle in between. Here, we only report on the observations made along the Sun-comet direction and the perpendicular direction. In addition to the spectra, images were made at the beginning of each night in broad band filters to study the dust coma of the comet. Table 1 provides an overview of the spectroscopic observing sequence for each night.

All frames taken with FORS 2 showed a coherent noise pattern which had to be removed. This noise pattern had a low frequency contribution parallel to the wavelength axis and a high frequency component parallel to the spatial direction. The low-frequency component was basically constant over each night and could be well determined from bias frames, where it was clearly visible. For the high-frequency component parallel to the spatial direction the investigations showed, however, a slight variation in frequency during the night. This noise component was determined using unexposed edges of the CCDs of FORS 2 in each single exposure. A Fourier filter method was applied for both noise components to identify and remove the noise. Then, the standard CCD reduction including bias subtraction and flat-fielding was performed. Some straylight contribution was found in frames with high exposure level. Again, the "non-exposed" edges of each frame could be used to determine the level of the straylight in each spectrum, which was then subtracted. Since no "unexposed edges" are present in data taken with FORS 1, a straylight correction could not be done for spectra taken on July 10/11 and 11/12.

The spectra were wavelength calibrated, sky background subtracted and corrected for extinction. For the sky background subtraction, separate sky frames taken through the night were used since the cometary coma fills the entire slit length. Absolute flux calibration was performed using spectroscopic standard stars observed prior to and after the comet observations. Observations during all nights, except during the night of July 06/07, were obtained under photometric conditions. To subtract the continuum emission caused by scattered solar light on the cometary dust particles in the coma, a solar catalog spectrum (Kurucz et al. 1984) was convolved with a Gaussian instrumental profile to the resolution of our observations and then fitted to the data in each row by a polynomial fit. An example of calibrated and continuum subtracted spectra taken before and after impact is shown in Fig. 1.

3. Results

3.1. Comparison of the pre- and post-impact spectra

In Fig. 1 spectra from the sunward side of the nucleus are shown after continuum subtraction. The emission lines usually present in optical comet spectra are detected, caused by CN, C_3, C_2 and NH_2 radicals. No emissions of H_2O^+ or CO^+ were seen.

To investigate whether new emission lines appeared after the impact of the spacecraft into the comet, we compared spectra taken before and after the event. To enhance the signal-to-noise ratio in the reference before impact, all spectra taken on July 3/4 were co-added. After impact, the ejecta cloud moves through the field-of-view and only individual spectra were used for comparison. All gas emission lines have increased in intensity (Fig. 1) after impact. However, no new emissions were present, and thus, no new molecules have been detected.

3.2. Spatial gas and dust profiles

Figure 2 shows the intensity distribution of the continuum, caused by solar light scattered by dust particles, along the slit parallel to the Sun-comet line. Two profiles are shown for the night of July 04/05 and one for all other nights. In Fig. 3, the radial continuum intensity profiles along the perpendicular direction are shown. The ejected dust cloud can be seen in the slit after impact in the sunward direction and 270° direction

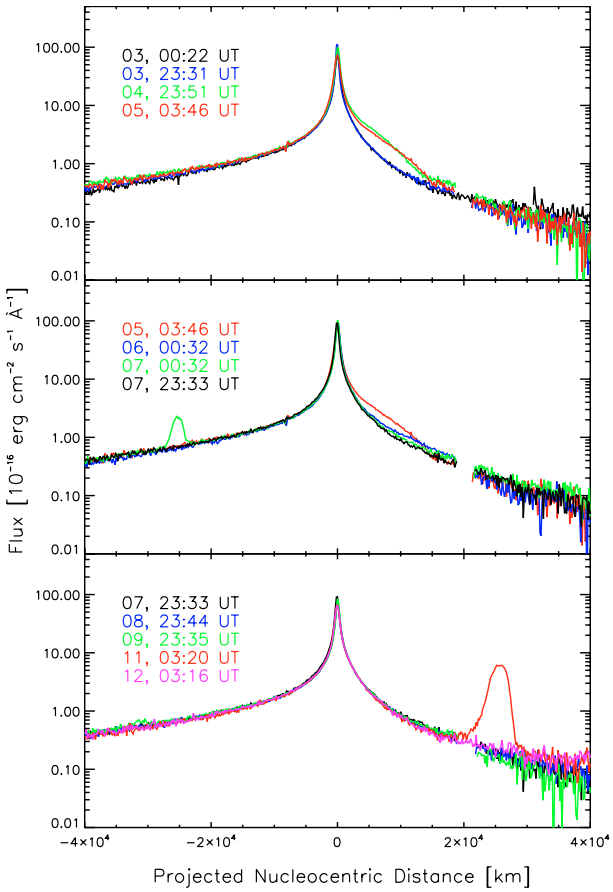

Fig. 2. Continuum flux along the Sun-comet line, measured at 5540 Å to 5575 Å. The different colors give the profiles at different nights. Isolated peaks in the profiles are caused by stars within the slit. Positive distance is counted towards the projected solar direction, negative in the antisolar direction.

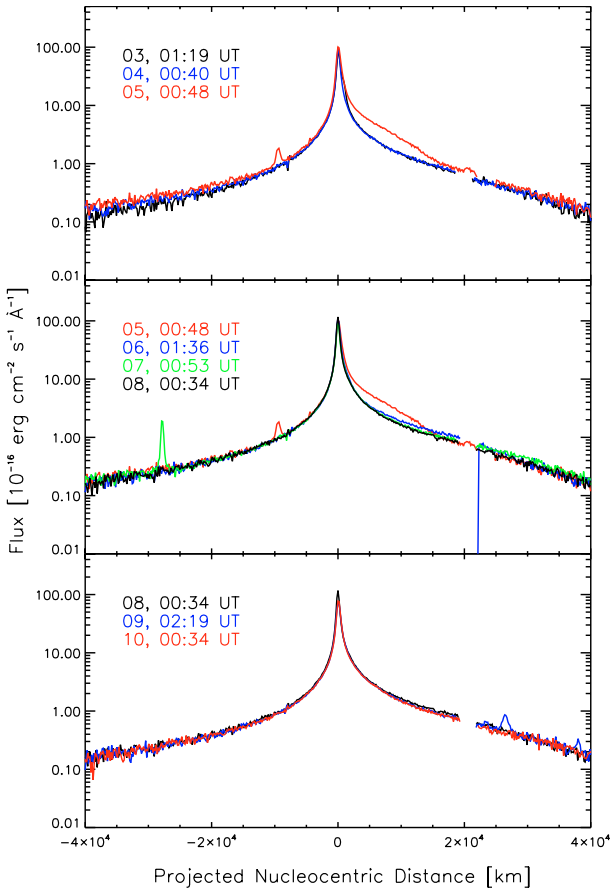

Fig. 3. Continuum flux perpendicular to the Sun-comet line, measured at 5540 Å to 5575 Å. The different colors give the profiles at different nights. Isolated peaks in the profiles are caused by stars within the slit. Positive distance is counted towards the 270° direction, negative in the 90° direction.

measured with respect to the projected solar direction. The cloud moves and expands along both directions. After five days the cloud vanished and the coma is back to an intensity profile similar to pre-impact. No change in the intensity profile is seen in the 90° and 180° directions.

The corresponding spatial profiles in the light of CN emission (violet system at 3875 Å) are shown in Figs. 4 and 5. Like in the continuum profiles, a cloud of ejected material moves in the sunward direction after impact. However, the CN cloud is visible in all directions (0°, 90°, 180°, and 270°) already 18 h after impact, again expanding and diluting in the subsequent nights. The fast lateral expansion of gas molecules in the coma causes the gas cloud to spread around the nucleus quickly. The long-slit spectra indicate that then a shell-like cloud of gas molecules expands around the nucleus. Four days after impact, the cloud has diluted and is visible just by a higher intensity profile in comparison to pre-impact. Again, at the end of our observing period the CN profile is back to pre-impact conditions.

3.3. Variations with rotation period

We notice another difference between the continuum and gas intensity profiles. After the impact cloud has been ejected, the intensity in the continuum remains constant in the innermost coma near the nucleus. In the light of CN, however, it rises again on July 6 (Fig. 4). Since the sky conditions of that night were non-photometric, it remains unknown whether the observed increase is indeed caused by an increased cometary activity. Then, the CN intensity at the nucleus position is going back to the pre-impact value. In order to study short-term variations, we investigated the brightness in the inner coma. Figure 6 shows the integrated flux over the inner pixels around the nucleus, as measured in the spectra of the 0°–180° direction. Because the pixels at and near the nucleus position are most affected by any possible mismatch between the fitted underlying continuum and the spectra, the innermost 7 pixels have been excluded. Then the adjacent 20 pixels (5″) on each side have been summed. This approach was chosen to minimize the influence of the impact cloud. The resulting integrated CN flux around the nucleus is also shown in Fig. 7, phased with the rotation period of the comet and normalized to the mean flux value. The rotation period was taken as (40.832 ± 0.33) h (A'Hearn et al. 2005). The data points in the night following the impact (July 04/05) are higher than intensities obtained on other nights at similar rotational phases. The most likely explanation is the increase in CN activity due to the impact cloud, which is also seen in Fig. 4 and which fades during our observing period.

At small rotation phases, the CN flux is increased by about 30% compared to the levels at larger phase (>0.6). Unfortunately, the data points on July 05/06 have a large error because this night was not photometric. The data points of July 07/08 are also enhanced and show a clear decrease in

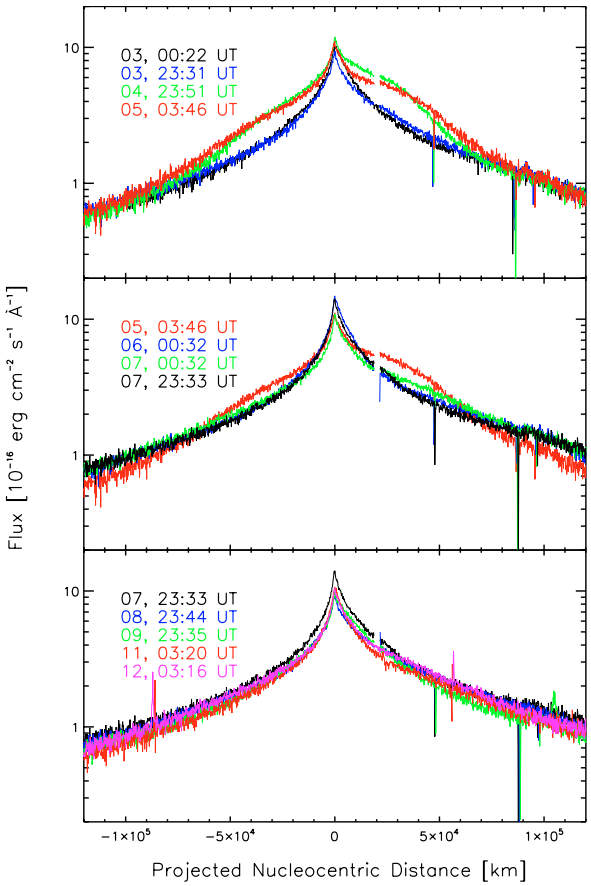

Fig. 4. CN emission flux along the Sun-comet line for different nights. Positive distance values are counted in the projected solar direction, negative values in the antisolar direction.

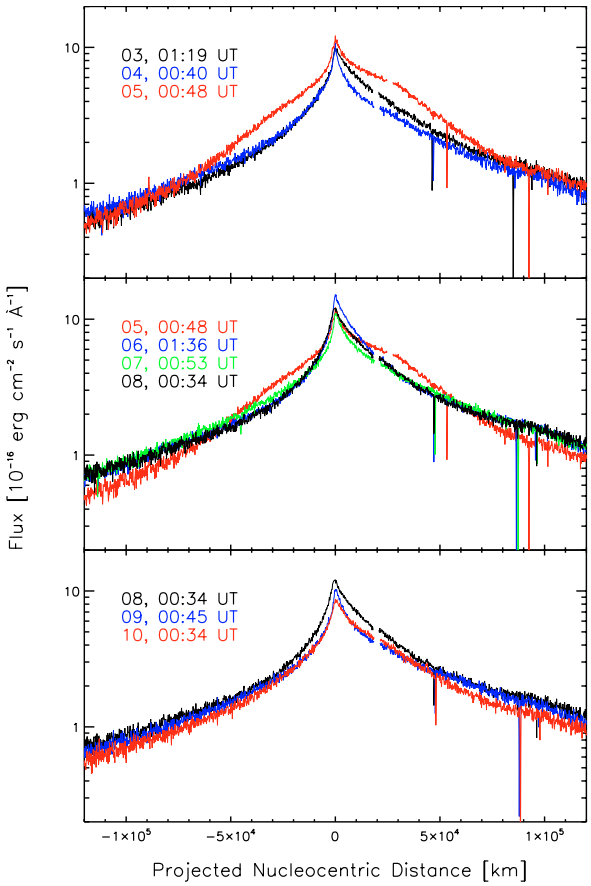

Fig. 5. CN emission flux perpendicular to the Sun-comet line for different nights. Positive distance values are counted in the 270° direction, negative values in the 90° direction.

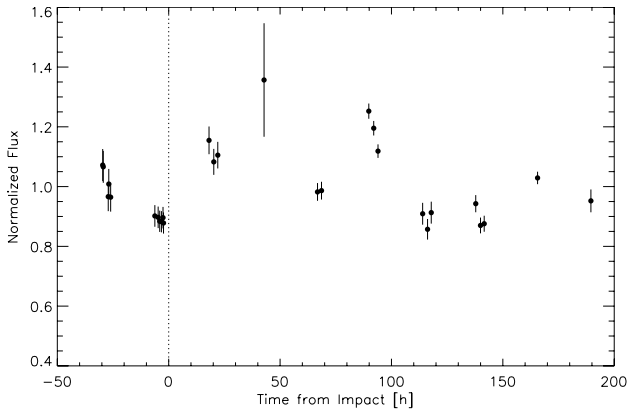

Fig. 6. CN line flux in the inner coma (±5.8″ around the nucleus excluding the inner 1.8″) over time. The values displayed are taken at the 0°–180° slit orientation. The points or groups of points belong to the nights from July 02/03 to July 11/12, 2005.

intensity over the night with increasing rotational phase angle. The observed intensity variation fits to the proposed rotational modulation found from small aperture high-spectral resolution observations obtained at VLT UT2 using UVES (Jehin et al. 2006). This variation, therefore, may be caused by an active area on the nucleus surface rotating in and out of sunlight, which was already present before impact. However, again it is unfortunate that data at small phase angles prior to the impact are not covered by our observations. We therefore can not exclude that we still see the effect of the impact cloud. Such an interpretation would be supported by the low flux level observed at small phase angles on July 10/11, a time period when the spatial profiles show that the impact cloud has already been diluted (Fig. 4). However, since the aperture used for the determination of the data points in Fig. 7 is very small, the ejecta cloud is providing a substantial contribution to the flux in the aperture for at most two days after impact. Therefore, small aperture observations like performed with UVES or in our small integration window should be less sensitive to the impact cloud. By comparison, the wider angle observations of Schleicher et al. (2006) show a stronger contribution from the impact cloud. In such data, therefore, rotational flux variations are diluted. To definitely conclude on the effect of rotational modulation, data at different phase angles and observing times from different sites must be combined in future.

3.4. Expansion velocities

We measured the projected expansion velocities of the dust and gas ejecta cloud. This was done by determining the projected nucleocentric distance where the intensity profiles of the cloud equals the background coma (see Figs. 2–5). The projected mean expansion velocities are given in Table 2. The velocity of the outermost part of the impact gas cloud can be determined only in the night after impact, before the cloud expands beyond the edges of the slit and dilutes. The lower dust velocity can also be determined in following nights. In the night of July 05/06, the tip of the dust cloud was within the gap between the two CCDs of FORS 2 and an accurate estimate of the dust expansion velocity was therefore not possible. In the

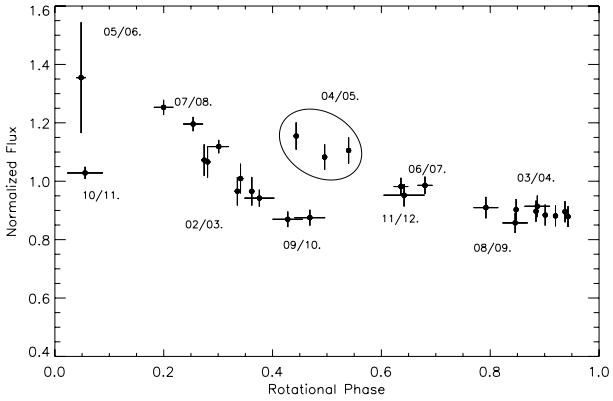

Fig. 7. CN line flux over rotational phase. The values displayed are taken at the 0°−180° slit orientation. Phase 0 corresponds to the impact time (July 04, 05:52 UT). The night of July 05/06 was non-photometric and the real errors may be even larger. The data from the night of July 04/05 include a significant contribution from the impact cloud and therefore are enhanced compared to data from the undisturbed coma at similar rotational phase.

Table 2. Projected mean expansion velocities of the outermost part of the dust and gas cloud. Δt gives the time since impact and p the projected distance from the nucleus of the outermost detectable part of the impact cloud. PA lists the position angle at which the measurement was done, with respect to the projected solar direction.

PA	date, time	Δt [s]	p [10^4 km]	v [km s^{-1}]
		CN		
0°	July 4, 23:50	65 182	$7.50^{+0.25}_{-0.25}$	$1.15^{+0.04}_{-0.04}$
180°	July 4, 23:50	65 182	$7.75^{+0.23}_{-0.38}$	$1.19^{+0.04}_{-0.06}$
90	July 5, 00:48	68 628	$7.78^{+0.33}_{-0.15}$	$1.15^{+0.05}_{-0.02}$
270	July 5, 00:48	68 628	–	–
0°	July 5, 01:58	72 861	$8.45^{+0.25}_{-0.57}$	$1.16^{+0.03}_{-0.08}$
180°	July 5, 01:58	72 861	$8.86^{+0.51}_{-0.38}$	$1.22^{+0.07}_{-0.05}$
0°	July 5, 03:46	79 334	$8.83^{+0.62}_{-0.21}$	$1.11^{+0.08}_{-0.03}$
180°	July 5, 03:46	79 334	$9.89^{+0.18}_{-0.39}$	$1.25^{+0.02}_{-0.05}$
		Dust		
270°	July 5, 00:48	68 628	$2.53^{+0.12}_{-0.36}$	$0.37^{+0.02}_{-0.05}$
0°	July 5, 01:58	72 861	$1.51^{+0.13}_{-0.15}$	$0.21^{+0.02}_{-0.02}$
0°	July 5, 03:46	79 334	$1.56^{+0.16}_{-0.13}$	$0.20^{+0.02}_{-0.02}$
270°	July 6, 01:36	157 935	$3.04^{+0.23}_{-0.38}$	$0.19^{+0.02}_{-0.02}$
0°	July 7, 00:32	240 477	$2.53^{+0.13}_{-0.15}$	$0.10^{+0.01}_{-0.01}$
270°	July 7, 00:53	241 760	$4.99^{+0.35}_{-1.90}$	$0.21^{+0.01}_{-0.08}$
0°	July 7, 02:20	246 965	$2.51^{+0.18}_{-0.23}$	$0.10^{+0.01}_{-0.01}$
270°	July 7, 03:01	249 430	$4.00^{+1.10}_{-0.45}$	$0.16^{+0.04}_{-0.02}$

following night, the dust velocity could be estimated again. It shows a clear decrease from night to night, which is caused by radiation pressure starting to act efficiently on the dust particles, accelerating them anti-sunward. On July 07/08 and later the dust cloud is too diluted to allow for a clear velocity determination. As expected from the influence of radiation pressure, the deceleration along the sunward direction is more efficient than along the 270° direction.

In addition, the velocity of the projected center of the CN cloud was determined on July 04/05 and July 05/06. When determing the position of the center of the impact cloud, the geometric dilution of the cloud while moving to larger nucleocentric distances has to be taken into account. For a steady-state coma, one would expect a decrease of the column density, and thus the observed line brightness, according to ρ^{-1}, when ρ is the projected nucleocentric distance. The expansion of the gas cloud resulting from the Deep Impact event is a transient phenomenon, and therefore probably not following a ρ^{-1} dependency. Since the distribution of the cloud material with time and nucleocentric distance is not known, in this work a weighting of the measured line flux with ρ^{-2} is applied as a first guess. Each line flux value along the radial intensity profiles was multiplied by the square of its distance to the nucleus position. If a larger power of ρ is used for correction, the derived velocities of the center of the cloud would be lower. Then, a Gaussian profile was fitted to the resulting corrected cloud and the position of the center of the Gaussian was assumed to be the projected center of the CN cloud. The derived radial positions and corresponding velocities of the center of the CN cloud are given in Table 3.

Table 3. Projected mean expansion velocities of the center of the CN gas cloud. Δt gives the time since impact and p the projected distance from the nucleus. PA lists the position angle at which the measurement was done, with respect to the projected solar direction.

PA	date, time	Δt [s]	p [10^4 km]	v [km s^{-1}]
0°	July 4, 23:50	65 182	3.75 ± 0.30	0.58 ± 0.05
180°	July 4, 23:50	65 182	4.13 ± 0.30	0.63 ± 0.05
90°	July 5, 00:48	68 628	3.95 ± 0.37	0.58 ± 0.05
270°	July 5, 00:48	68 628	4.91 ± 0.31	0.72 ± 0.05
0°	July 5, 01:58	72 861	4.35 ± 0.32	0.60 ± 0.04
180°	July 5, 01:58	72 861	4.62 ± 0.30	0.63 ± 0.04
0°	July 5, 03:46	79 334	4.78 ± 0.32	0.60 ± 0.04
180°	July 5, 03:46	79 334	5.04 ± 0.30	0.64 ± 0.04
0°	July 6, 00:32	154 083	9.91 ± 1.00	0.64 ± 0.07
180°	July 6, 00:32	154 083	10.55 ± 1.04	0.69 ± 0.07

3.5. Quantitative investigation of the CN ejecta cloud

The next step of investigation is to quantify the increase in gas emission due to the impact. First, we concentrated on the longer term effects and used a Haser model (Haser 1957) to compute the gas production rate of CN before and 5−8 days after impact. At this time, the ejecta cloud had already left the field of view and a Haser model was a good approximation of the coma column density. Scale lengths of CN were determined from the spatial coma intensity profiles. Because of the asymmetry of the coma, we treated the radial intensity profiles along each position angle of the slit separately. Because of the rather long daughter scale length for CN, it could be determined only from one spectrum where the comet was close to the edge of the slit. The destruction scale length derived was then assumed to be the same for both sides and all spectra. The resulting scale lengths for parents, l_p, and daughters, l_d, for the comet at a heliocentric distance of 1.51 AU are:

$l_\mathrm{p} = (5.18 \pm 1.32) \times 10^4$ km, sunward

$l_\mathrm{p} = (4.13 \pm 0.62) \times 10^4$ km, tailward

$l_\mathrm{d} = (12.4 \pm 9.3) \times 10^5$ km.

These scale lengths compare well with those derived in the literature (e.g. A'Hearn et al. 1995; Cochran et al. 1992; Newburn & Spinrad 1989) when normalized to 1 AU heliocentric distance. A g-factor of 1.05×10^{-13} erg s^{-1} molecule^{-1} for the CN radical at a heliocentric distance of 1.51 AU was used. This value was obtained by scaling of the value for zero radial velocity given by Schleicher (1983) to the heliocentric distance of the observations. The variation of the radial heliocentric velocity component over the observing period is small (see Table 1) and was neglected. A nucleus radius of 3.0 km (A'Hearn et al. 2005) was assumed. A gas expansion velocity of 1.0 km s^{-1} was used for

Table 4. CN gas production rates determined using a Haser model. Columns give the values derived from spatial profiles along the different position angles with respect to the projected solar direction. All values are in [10^{24} s^{-1}].

date	Q(CN) 0°	Q(CN) 180°	Q(CN) 90°	Q(CN) 270°
July 02/03	10.8 ± 0.4	8.4 ± 0.9	7.3 ± 0.3	16.6 ± 0.8
July 03/04	13.7 ± 0.4	8.1 ± 0.3	8.2 ± 0.2	13.2 ± 0.3
July 08/09	15.8 ± 2.9	10.2 ± 0.3	9.7 ± 0.5	15.8 ± 0.6
July 09/10	12.8 ± 1.3	9.1 ± 0.3	8.1 ± 0.1	15.4 ± 0.5
July 10/11	10.4 ± 0.9	7.0 ± 0.3	–	–
July 11/12	14.6 ± 1.3	11.1 ± 0.5	9.3 ± 0.3	16.3 ± 0.6

the determination of the CN production rate for easy comparison with other publications. Table 4 gives the Haser CN production rates before impact and 5−8 days after impact for comparison. Within error bars, the production rates a few days after impact are similar to the pre-impact conditions on the sunward side. Along the tail direction some increase due to the ejecta cloud or coma asymmetries may still be seen on July 08/09, but decreasing in the following nights.

During the days immediately after impact we see the ejecta cloud travelling outwards. Obviously, it is not possible to use a steady-state Haser model to derive the production rates of the comet at this time. Since the details of the observed transient coma phenomenon, such as the distribution of the CN parents and their velocities, are unknown, a simplistic approach is chosen. As long as the complete CN cloud lies within the slit used for observations, as it was the case in the night of July 04/05, the total number of CN molecules in the cloud can be estimated assuming isotropic cloud expansion. It is further assumed that all CN parent molecules in the ejecta cloud were released at the same time, during impact. The approximation of the same age for all CN parent molecules in the impact cloud is justified as long as the time of release of the parent molecules is short compared to the observational time scale.

If a simple two step chemical reaction network is assumed, with one reaction for the formation of CN and reaction rate coeffient k_p, and one for its destruction with k_CN, the total number of CN molecules in the impact cloud as a function of time is obtained from the solution of the differential equations

$$\frac{\mathrm{d}N_\mathrm{p}}{\mathrm{d}t} = -k_\mathrm{p} N_\mathrm{p} \quad (1)$$

$$\frac{\mathrm{d}N_\mathrm{CN}}{\mathrm{d}t} = k_\mathrm{p} N_\mathrm{p} - k_\mathrm{CN} N_\mathrm{CN} \quad (2)$$

with the initial conditions $N_\mathrm{p}(t = t_0) = N_\mathrm{p}^\mathrm{impact}$ and $N_\mathrm{CN}(t = t_0) = 0$. Here, t_0 denotes the impact time and $N_\mathrm{p}^\mathrm{impact}$ the number of CN parent molecules set free by the impact event. The solution of the differential equations yields

$$N_\mathrm{CN}(t) = N_\mathrm{p}^\mathrm{impact} \frac{k_\mathrm{p}}{k_\mathrm{CN} - k_\mathrm{p}} \left[\mathrm{e}^{-k_\mathrm{p}(t-t_0)} - \mathrm{e}^{-k_\mathrm{CN}(t-t_0)} \right]. \quad (3)$$

The rate coefficients are derived from the Haser scalelengths determined in the nights before impact by:

$$k_\mathrm{p} = \frac{v}{l_\mathrm{p}}, \qquad k_\mathrm{CN} = \frac{v}{l_\mathrm{CN}}. \quad (4)$$

We set v equal to the projected expansion velocity of the gas ejecta cloud determined from our spatial CN profiles. The mean value derived from Table 2 is 1.19 ± 0.07 km s^{-1}. We use this set of equations to derive the number of parent molecules released during impact, $N_\mathrm{p}^\mathrm{impact}$. The number of CN molecules in the ejecta cloud, N_CN, can be derived from our observations under the assumptions outlined above. To do so, the emission profile of CN obtained in the night before impact was subtracted from the profiles of the night after impact. Then the resulting intensity profile is integrated over the cloud. The number of CN and the derived parent molecules are given in Table 5.

Table 5. Number of CN radicals within the impact cloud and the derived number of parent molecules released by the impact. The values derived from spectra in different directions are given, assuming a spherically symmetric coma, respectively. $t - t_0$ gives the time since impact. N_CN corresponds to the total number CN molecules in the cloud, N_p is the number of parent molecules, most likely HCN, derived from Eq. (3). All values are given in [10^{29} molecules].

Date [UT]	PA	N_CN	$t - t_0$ [s]	N_p
July 4, 23:50	0°	3.27 ± 0.47	65 182	4.63 ± 0.73
	180°	2.33 ± 0.35		2.75 ± 0.43
July 5, 00:48	90°	2.70 ± 0.50	68 628	3.27 ± 0.62
	270°	2.40 ± 0.35		2.90 ± 0.44
July 5, 01:58	0°	3.38 ± 0.66	72 861	4.57 ± 0.94
	180°	2.50 ± 0.48		2.88 ± 0.57
July 5, 03:46	0°	3.88 ± 0.68	79 334	5.09 ± 0.94
	180°	2.95 ± 0.49		3.36 ± 0.58

4. Summary and discussion

The impact of the Deep Impact spacecraft into comet P/Tempel 1 led to the formation of a crater on its surface and an ejecta cloud of gas and dust expanding into the cometary coma (A'Hearn et al. 2005). Our observations of this event performed by long-slit spectroscopy at the ESO VLT prior to and post impact showed the ejecta cloud in the light of the radicals seen in optical spectra of comets and in the continuum light caused by solar radiation scattered on dust particles. It was discussed whether new molecules would become visible from fresh sub-surface ice layers of the nucleus or formed by the high density and temperature conditions during the impact. Our observations could, however, not show any new emission lines after impact.

The ejecta cloud was covered in the long-slit spatial profiles and was followed until 8 days after the impact event. The cometary coma, however, showed conditions similar to pre-impact already 5–6 days after the event. This is supported by the spatial CN and dust distribution (Figs. 2–5) and a quantitative comparison of CN production rates (Table 4) of 5–7 days after the impact event with their values before impact. The projected expansion velocity of the CN gas cloud is around 1.2 km s^{-1} for the outermost part (see Table 2) on the day after impact. The center of the cloud moves with a mean projected velocity of about 0.6 km^{-1}. The slower dust cloud moved with about 0.21 km s^{-1} in the projected solar direction within one night after impact, and decreased to a mean velocity of 0.10 km s^{-1} until July 07, showing the effect of the solar radiation pressure. In the 270° direction, the projected dust velocities are somewhat higher, decreasing from about 0.37 km s^{-1} to 0.21 km s^{-1} in the same time.

We estimated the total number of CN parent molecules ejected by the impact event assuming a two-step formation and destruction model of CN to take into account the chemical processes in the cloud from impact time up to our observations. We assume all parent molecules released at the same time during

the impact and isotropic conditions in the coma. With these assumptions we estimate a total of about $(3.7 \pm 1.9) \times 10^{29}$ parent molecules ejected by Deep Impact. Assuming HCN as the main parent species, this would correspond to a mass of (17.5 ± 5.4) tonnes. The impact event provided a total kinetic energy of 1.93×10^{10} J. With a sublimation enthalpy of 35.6 kJ/mol for HCN (Stephenson & Malanowski 1987), a total of 3.26×10^{29} molecules of HCN could be sublimated due to the impact event if all energy would be used for the sublimation of HCN only. This value is of the same order of magnitude as the number of CN parents produced by the impact. Since HCN is only a minor component of cometary nuclei (for 9P/Tempel 1, an abundance ratio HCN/H_2O of (0.18 ± 0.06)% was determined (Mumma et al. 2005)), the kinetic energy provided by the impact spacecraft is not sufficient to explain the observed amount of volatiles released due to the impact. Sublimating icy grains ejected into the coma by the impact event are a likely explanation for the observed amount of volatiles in the impact cloud. The assumption of an instantaneous release of all parent species may nevertheless be justified since studies of the dust cloud (Schleicher et al. 2006) indicate typical grain sizes below about 2.5 μm. If icy particles also have such low sizes and contain dark material, the complete sublimation of the grains takes less than 30 min (Beer et al. 2006) at heliocentric distances between 1–2 AU. Therefore, the approach chosen may provide an approximation of the total amount of sublimated HCN.

Acknowledgements. The authors warmly thank Jean Manfoid for his support during the observations with FORS1.
C. Sterken acknowledges financial support from the Belgian Fund for Scientific Research (FWO).

References

A'Hearn, M. F., Millis, R. L., Schleicher, D. G., et al. 1995, Icarus, 118, 223
A'Hearn, M. F., Belton, M. J. S., Delamere, W. A., et al. 2005, Science, 310, 258
Beer, E. H., Podolak, M., & Prialnik, D. 2006, Icarus, 180, 473
Cochran, A. L., Barker, E. S., Ramseyer, T. F., & Storrs, A. D. 1992, Icarus, 98, 151
Haser, L. 1957, Bulletin de la Societe Roaly des Sciences de Liege, 43, 740
Jehin, E., Manfroid, J., Hutsemékers, D., et al. 2006, ApJ, 641, 145
Kurucz, R. L., et al. 1984, Solar flux atlas from 296 to 1300 nm (Sunspot, New Mexico: National Solar Observatory)
Meech, K., Ageorges, N., A'Hearn, M. F., et al. 2005, Science, 310, 265
Mumma, M. J., DiSanti, M. A., Magee-Sauer, K., et al. 2005, Science, 310, 270
Newburn, R. L., & Spinrad, H. 1989, AJ, 97, 552
Stephenson, R. M., & Malanowski, S. 1987, Handbook of the Thermodynamics of Organic Compounds (Elsevier)
Schleicher, D. G. 1983, Ph.D. Thesis, University of Maryland
Schleicher, D. G., Barnes, K. L., Baugh, N. F., et al. 2006, AJ, 131, 1130

Online Material

Table 1. Observing log including all long-slit spectra. The Table provides the date and time of each observation, the exposure time, exp, and the wavelengths range, $\Delta\lambda$, covered in each spectrum. The position angle of the slit, PA, is measured from the projected solar direction towards North. Observations marked with * were done using FORS 1, others were performed with FORS 2. †Night not photometric.

Time [UT]	exp [s]	$\Delta\lambda$ [nm]	PA [°]	r_h [AU]	v_r [km s^{-1}]	Δ [AU]	solar PA [°]
July 3, 00:09	600	370–620	0, 180				
July 3, 00:21	900	370–620	0, 180				
July 3, 00:40	900	610–920	0, 180				
July 3, 01:19	900	370–620	90, 270				
July 3, 01:43	900	370–620	135, 315	1.51	−0.38	0.88	291.7
July 3, 02:14	900	370–620	45, 225				
July 3, 02:36	900	370–620	0, 180				
July 3, 02:49	900	370–620	0, 180				
July 3, 03:11	900	370–620	90, 270				
July 3, 03:40	900	370–620	0, 180				
July 3, 23:31	900	370–620	0, 180				
July 3, 23:49	900	610–920	0, 180				
July 4, 00:40	900	370–920	90, 270				
July 4, 01:00	900	370–620	0, 180				
July 4, 01:21	900	370–620	90, 270				
July 4, 01:42	900	370–620	0, 180	1.51	−0.15	0.89	291.4
July 4, 02:07	900	370–620	90, 270				
July 4, 02:28	900	370–620	0, 180				
July 4, 02:50	900	370–620	90, 270				
July 4, 03:11	900	370–620	0, 180				
July 4, 03:27	600	370–620	0, 180				
July 4, 23:50	900	370–620	0, 180				
July 5, 00:07	900	610–920	0, 180				
July 5, 00:48	900	370–620	90, 270				
July 5, 01:13	900	370–620	135, 315				
July 5, 01:36	900	370–620	45, 225	1.51	−0.03	0.90	291.3
July 5, 01:58	900	370–620	0, 180				
July 5, 02:22	900	370–620	135, 315				
July 5, 03:22	900	370–620	135, 315				
July 5, 03:46	900	370–620	0, 180				
July 6, 00:32	900	370–620	0, 180				
July 6, 00:53	900	610–920	0, 180				
July 6, 01:36	900	370–620	90, 270	1.51	0.09	0.90	291.1 †
July 6, 02:00	900	370–620	135, 315				
July 6, 02:30	606	370–620	45, 225				
July 6, 02:57	600	370–620	45, 225				
July 7, 00:32	900	370–620	0, 180				
July 7, 00:53	900	370–620	90, 270				
July 7, 01:17	900	370–620	135, 315				
July 7, 01:39	900	370–620	45, 225	1.51	0.20	0.91	291.0
July 7, 02:20	900	370–620	0, 180				
July 7, 02:39	900	610–920	0, 180				
July 7, 03:01	900	370–620	90, 270				
July 7, 03:24	900	370–620	135, 315				
July 7, 23:33	900	370–620	0, 180				
July 7, 23:52	900	610–920	0, 180				
July 8, 00:34	900	370–620	90, 270				
July 8, 00:58	900	370–620	135, 315				
July 8, 01:24	900	370–620	45, 225	1.51	0.32	0.91	290.9
July 8, 01:46	900	370–620	0, 180				
July 8, 02:30	900	370–620	90, 270				
July 8, 02:53	900	370–620	135, 315				
July 8, 03:18	900	370–620	45, 225				
July 8, 03:41	900	370–620	0, 180				

Table 1. continued.

Time [UT]	exp [s]	$\Delta\lambda$ [nm]	PA [°]	r_h [AU]	v_r [km s^{-1}]	Δ [AU]	solar PA [°]
July 8, 23:44	900	370–620	0, 180				
July 9, 00:03	900	610–920	0, 180				
July 9, 00:45	900	370–620	90, 270				
July 9, 01:11	900	370–620	135, 315				
July 9, 01:32	900	370–620	45, 225	1.51	0.44	0.92	290.7
July 9, 01:56	900	370–620	0, 180				
July 9, 02:19	900	370–620	90, 270				
July 9, 02:42	900	370–620	135, 315				
July 9, 03:03	900	370–620	45, 225				
July 9, 03:36	900	370–620	0, 180				
July 9, 23:34	900	370–620	0, 180				
July 9, 23:54	900	610–920	0, 180				
July 10, 00:34	900	370–620	90, 270				
July 10, 00:56	900	370–620	135, 315				
July 10, 01:20	900	370–620	45, 225	1.51	0.55	0.93	290.5
July 10, 01:42	900	370–620	0, 180				
July 10, 02:05	900	370–620	90, 270				
July 10, 02:28	900	370–620	135, 315				
July 10, 02:50	900	370–620	45, 225				
July 10, 03:22	900	370–620	0, 180				
July 11, 03:20*	900	370–580	0, 180	1.51	0.67	0.93	290.5
July 12, 03:16*	900	370–580	0, 180	1.51	0.78	0.94	290.3
July 12, 03:40*	600	370–580	90, 270				